Vascular Carbon/Carbon Composites for Concentrated Solar Power

Jose C. Cordeiro Jr.[1], Matt Zuzelski[2], Mark H. Olima[3], Daniel W. Crunkleton[1], Todd Otanicar[2], Hema Ramsurn[1], Michael W. Keller[3]

[1] *Russell School of Chemical Engineering, University of Tulsa, 800 S Tucker Dr, Tulsa, OK, USA*

[2] *Mechanical and Biomedical Engineering, Boise State University, 1910 University Drive, Boise, ID, USA*

[3] *Department of Mechanical Engineering, University of Tulsa, 800 S Tucker Dr, Tulsa, OK, USA*

Abstract

Due to their exceptional mechanical and thermal properties under high temperature conditions, for the first time, a novel vascular (embedded channels) Carbon/Carbon (C/C) composite was developed for use as a modular concentrated solar power (CSP) gas receiver. The fabrication process involves the combination of the vaporization of sacrificial component (VaSC) technique with conventional methods to produce C/C composites with well preserved channels. Different heat treatments were evaluated together with X-ray diffraction (XRD) analysis to determine optimal fabrication conditions that maintains the material and channel's integrity. Mechanical testing confirms that structural integrity is maintained, with statistical analyses indicating no compromise in flexural strength or modulus. This research introduces an innovative pathway for efficient CSP gas receivers, which can bridge the gap towards improved energy generation efficiency in next-gen CSP plants through higher operating temperatures with the use of C/C composites.

Keywords: Carbon/Carbon composites, vascular, concentrated solar power.

1. Introduction

Concentrated solar power (CSP) systems work by focusing sunlight into a receiver, which in turn heats a working fluid that is later used with power cycles to generate electricity [1]. A major advantage of CSP over photovoltaic cells is the implementation of thermal storage systems, usually in the form of molten salt tanks, which are used as a source of heat during the night and provide CSP with on-demand energy generation capabilities [2]. The receiver operating

Email address: hema-ramsurn@utulsa.edu (Hema Ramsurn[1])

temperature is a major contributor to the plant's overall efficiency. The U.S. DoE (United States Department of Energy) GEN3 road map [3] has identified the use of sCO_2 (super-critical carbon dioxide) Brayton-cycles and receiver operating temperatures of above 800 °C as integral parts of the next generation of CSP plants. Recent research has shown that the use of receiver modules with channels fabricated from nickel alloys has the potential of achieving nearly 90% global receiver efficiency based on simulated solar testing [4]. Although these results are impressive, some technical challenges still need to be overcome before adoption. At the GEN3 temperatures (> 800 °C), mechanical performance is critical as creep within the modules becomes a significant issue when considering the use of high-performance metal alloys, such as Inconel 718 [4]. Here we present the fabrication and characterization of a novel, vascular C/C composite, intended for use as central receiver modules. By taking advantage of their low CTE (coefficient of thermal expansion), C/C composites as the material of construction for CSP receivers allows for higher operating temperatures. When compared to Inconel 718, C/C composites offer comparable thermal conductivity (11 to 17 W m^{-1} K^{-1} for Inconel 718 [5]) while having a CTE of 0.1 to 0.6 $\times 10^{-6}$ K [6], which is two orders of magnitude lower than the CTE of Inconel 718 (13.2 to 14.6 $\times 10^{-6}$ K [5]). In addition, when compared to Inconel and its alloys, C/C composites are lightweight (1.5 to 2.5 g/cm^3[7]), potentially leading to decreased installation costs. As illustrated in Figure 1(a), a concentrated solar power gas receiver in a modular configuration is proposed, where each module (Figure 1(b)) will be made with a novel C/C composite with an embedded channel network through which super-critical carbon dioxide (sCO_2) will flow and be heated by the concentrated solar light. This approach has been previously proposed by our research group [8], where we demonstrated through computational fluid dynamics simulations that the new material (vascular C/C composites) are able to handle higher solar fluxes, taking into consideration material properties, heat transfer fluids, and different vascular designs. Results showed that a receiver fabricated with the proposed novel material can achieve thermal efficiencies above 90%, and up to 85% when considering realistic constrain limits, with regards to strain and heat flux.

Due to their exceptional properties and specialized fabrication method, C/C composites find niche applications in the aerospace industry (heat shield of re-entry vehicles and rocket nozzles) and in aviation (disk brakes of airplanes) [9, 7]. These composites are made of carbon fibers (CF), usually either pitch-based or PAN (polyacrylonitrile) based, that are surrounded by a

continuous carbonaceous matrix, hence the name "carbon/carbon" composites [10]. Pitch-based carbon fibers provide the highest modulus and thermal conductivity when compared to PAN-based CF, with the main drawback being a significant increase in cost. As the carbon source for the matrix, pitch or mesophase pitch [11, 12] are sometimes used due to their high carbon yields and ease of graphitization, but their high melting points (around 300 °C[12]) makes processing more challenging. On the other hand, the use of phenolic resins [13] provide comparable carbon yields while being much easier to process since they are available in the liquid state at room temperature. Heat treatments above 1000 °C convert the carbon source into the carbonaceous matrix [14, 15] that forms the C/C composite, in a process referred to as carbonization, that increases porosity and decreases density due to mass loss. As shown by Li et al. [16], using PAN-based CF and phenolic resin, prepared C/C composites had a final density of 1.54 g/cm^3 with an open porosity of 9.9%. Although, to achieve higher densities, the same resin precursor (such as a phenolic resin) can be used to re-infiltrate the carbonized material followed by re-carbonization, this would inevitably clog the channels of the proposed C/C composites. An alternative is to use chemical vapor infiltration (CVI), where a gaseous carbon source (e.g. methane) is cracked at high temperatures to deposit carbon on the surface of the pores [17, 12, 18, 19, 20, 21, 22, 23]. As reported by Ren et al. [23], C/C composites prepared using PAN-based CF achieved a density of 1.84 g/cm^3 when densifying with methane for 120 hours, showing that this approach can be used to produce high-density C/C composites. Zhang et al. [24] used highly graphitic pitch-based CF with a phenolic resin, followed by densification through CVI using propene, to produce highly heat conductive (maximum heat conductivity of 890 W m^{-1}K^{-1}) C/C composites with density of 1.72 g/cm^3 and open porosity of 16%. As a last step in the fabrication of C/C composites, graphitization above 2000 °C converts the matrix into a more crystalline graphite matrix, greatly improving thermal conductivity and tensile strength [25, 26]. The VaSC (vaporization of sacrificial components) technique [27] has been shown to be effective in the implementation of channels and vascular networks in composites and resin materials [28, 29]. These channels allow for intrinsic thermal management for batteries [30] and radiators of spacecraft components [31]. The use of PLA (polylactic acid) in VaSC allows for 3D printing to be used to obtain a desired channel network. PLA can be depolymerized above 295 °C under vacuum, or above 200 °C when catalyzed with tin(II) oxalate [27, 32] to leave a cleared channel network in its place. In this work, a prepreg with channels is first fabricated using the VaSC

technique, followed by multiple heat treatments to produce, for the first time, a C/C composite with an embedded channel network. The use of both PAN-based and pitch-based carbon fibers are evaluated, where a prepreg is first made using a resorcinol-added phenolic resin [33]. Because of their high carbon yield and aromatic nature, phenolic resins offer great advantages as a carbon matrix precursor for the fabrication of C/C composites. Acid and basic catalysts are commonly used to decrease curing times of resole phenolic resins. The addition of resorcinol instead is known to also be able to reduce curing times without potential contaminants from catalysts. In our previous work [33], it was demonstrated for the first time that the addition of resorcinol was able to reduce curing times by 71% without a detrimental effect to its carbon yield, which is an important factor for the fabrication of C/C composites. The 10 wt% resorcinol system has shown to be a transition between the phenol-formaldehyde and the more reactive resorcinol-formaldehyde curing reactions [33]. This approach maintained the embedded channels integrity without collapsing by allowing the resin to quickly B-stage cure (gel), greatly increasing its viscosity and providing more resistance to the compaction forces from the autoclave. To prevent clogging of the channels during densification, CVI with methane was used. The specimens are characterized with SEM (scanning electron microscopy), XRD (X-ray diffraction) analysis and three-point bending test.

2. Experimental

2.1. Materials

A commercially available phenolic resin was provided by Bakelite Chemicals. Resorcinol ($\geq$ 99 %) was acquired from BeanTown Chemical, and acetone (ACS grade) from VWR Chemicals. Nitrogen (99.999 %), argon (99.999 %), and methane (99.9 %) were obtained from Linde. Pitch-based carbon fibers were purchased from Mitsubishi Carbon, with twill weaving (K13C2U, 3K tow size, thermal conductivity of 620 W $m^{-1}K^{-1}$, fiber diameter of 9.6 μm, tensile strength of 3,800 MPa, and tensile modulus of 900 GPa) and unidirectional (K63712, 12K tow size, thermal conductivity of 140 W $m^{-1}K^{-1}$, fiber diameter of 11 μm, tensile strength of 2,600 MPa, and tensile modulus of 640 GPa). PAN-based carbon fibers were acquired from Toray (T700S with 12K tow size, thermal conductivity of 9.6 W $m^{-1}K^{-1}$, fiber diameter of 7 μm, tensile strength of 4,900 MPa, and tensile modulus of 230 GPa). A commercial C/C composite plate (FS240, with a flexural strength of 180 MPa and a flexural modulus of 45 GPA) was purchased

from Across USA, Inc. It is made up of bi-directional long fibers in a 0°/90°orientation. Samples from this plate were used as control.

The procedures and processing parameters for the fabrication of C/C composites with channels are summarized in Figure 2 and further described in sections 2.2 to 2.5. A detailed schematic diagram for the fabrication procedure is available in the supplementary information (Figure S1).

2.2. Prepreg with channels

The first step is to produce a cured prepreg (step 1 in Figure 2) using carbon fibers (either pitch or PAN-based) and a 10 wt% resorcinol-added phenolic resin as per our previous work [33]. Indeed, it was observed that curing of this resin with 10 wt% resorcinol involves multiple reactions that do not maintain a constant activation energy. Our published study [33] also demonstrated that among all models tested, the Vyazovkin method (VO) has proven to provide accurate isothermal curing predictions for this resorcinol-added phenolic resin system. Its algorithm friendly form allows for precise and fine calculations of activation energy as a function of conversion, allowing for very small isoconversional steps to be used, which also contributed to increase the precision of the method [33]. A sacrificial 3D printed PLA (polylactic acid) template for the desired channel network is placed in between the layers of carbon fibers, as shown in Figure 3. The PLA used has a 2.5 wt% added tin-oxide to act as a catalyst, facilitating and allowing the polymerization to be performed at 210 °C. The fiber layup, with the PLA channels (500 μm in diameter) in between, is then soaked with a resorcinol-added phenolic resin and placed inside a vacuum bag assembly. This assembly is illustrated by Figure 4(a), consisting of an outer vacuum bag, followed by a breather cloth and perforated peel ply. Sealant tapes are used to fix and seal the bag on top of an aluminum plate. The vacuum-bag assembly is then placed inside a stainless steel autoclave, as shown in Figure 4(b). The autoclave was designed and built in-house, rated for operation at 160 psi. A nitrogen line is used to pressurize the autoclave, which is also connected to a spring valve that automatically relieves gas to keep a constant pressure of 160 psi. A vacuum line with a controller is connected to the interior of the bag and aids in removing bubbles, while the nitrogen pressure provided by the autoclave acts on the exterior of the outer bag. The autoclave/vacuum-bag assembly is placed inside a temperature-controlled oven, rated for up to 150 °C. A thermocouple placed inside the autoclave measures the temperature throughout the experiment. For comparison purposes, prepregs were also prepared in a conventional out-of-autoclave fashion, where the vacuum bag assembly was

directly placed inside the temperature-controlled oven, without an autoclave.

In this work, curing of the prepregs was divided into two isothermal heating steps: (i) 50 °C for 12 hours to B-stage cure; and (ii) 130 °C for 12 hours to finalize C-stage curing. The prepreg is then sectioned using a diamond saw for further processing. Using a quartz tube furnace, the prepreg is heat treated at 290 °C for 24 hours under full vacuum (step 2 in Figure 2) to complete the VaSC process, depolymerizing the PLA and leaving behind a prepreg with the desired cleared channel network.

2.3. Carbonization and residual stress relief

The prepreg, now with the cleared channel network, is then carbonized at 1000 °C for 1 hour (step 3 in Figure 2) under argon atmosphere. With a carbon yield of 62.3 wt% [33], gas evolution during carbonization of the resin needs to be slow enough to prevent damage to the specimen, thus a heating rate of 1 °C/min was used. Due to matrix shrinkage, residual stresses develop between the carbon matrix and the carbon fibers. To relieve these stresses, an intermediate graphitization heat treatment at 2200 °C for 1 hour is performed (step 4 in Figure 2). A furnace with a graphite heating element (Carbolite Gero / LHT-200) under argon atmosphere is used, with a heating rate of 20 °C/min.

2.4. Densification through chemical vapor infiltration

Due to gas evolution during carbonization, the sample's porosity increases and its density decreases. Density is then increased by filling the pores with carbon, done in this work through CVI. Using a quartz tube furnace, methane is flowed at 200 mbar and 1000 °C to promote carbon deposition. The process is done through isothermal CVI, where the specimen is heated from the outside, creating a hotter sample surface where carbon usually tends to deposit faster. The vacuum assists in methane infiltration from the hotter outside surface into the composite before the deposition reaction occurs, providing a more homogeneous densification. The densification was done in 20 hour cycles (for a total of 60 hours), where the samples were then taken out after each cycle and ground to remove the carbon crust that forms from excessive carbon deposition at the surface, allowing for methane to better infiltrate the sample in the subsequent cycles.

2.5. Graphitization

Similar to the intermediate graphitization step performed in section 2.3, the densified specimen is heat treated at 2200 °C with a rate of 20 °C/min under an argon atmosphere (step 6 in Figure

2). Dwell times from 1 to 6 hours were used to evaluate the effect on graphitization degree and crystallinity. After this final heat treatment, a C/C composite with embedded channels is obtained.

2.6. Characterization and analysis

SEM (Helios 660 SEM) was extensively used to evaluate the morphology of the specimens during different stages of the fabrication process. NanoCT imaging was done to evaluate the integrity of the channels. Porosity and density were measured using the water absorption method, with standard deviation (SD) corresponding to three measurements on the same sample. Thermal conductivity was calculated based on measured thermal diffusivity with laser flash analysis (Linseis LFA1000) [8], and specific heat measured with DSC (differential scanning calorimetry, DSC 2500 TA-Instruments) analysis. XRD analysis was done to study heat treatment effects on the graphitization of the matrix. To investigate the effect of carbonization and graphitization on the matrix and on the carbon fibers, XRD analysis (Rigaku MiniFlex) was also done separately on powdered pitch and PAN-based carbon fibers, as well as powdered bulk samples of pure and resorcinol-added phenolic resins. Bulk matrix samples were prepared by adding the resin into silicone cylindrical mold and cured inside the autoclave at 50 °C for 12 hours, followed by 130 °C for 12 hours. The resin was then carbonized at 1000 °C for 1 hour, and graphitized at 2200 °C for 1h, and later for an additional 3h and 6h. The same carbonization and graphitization heat treatments were done to the carbon fibers. The d-spacing (d) was calculated by using the Bragg's law shown in Equation 1:

$$n\ \lambda = 2\ d\ sin\ \theta \tag{1}$$

where n is diffraction order ($n = 1$), λ is the radiation wavelength ($\lambda = 1.5406\ \mathring{A}$), θ is the Bragg angle. The crystallite size (L) was calculated with the Scherrer's equation shown in Equation 2:

$$L = \frac{K\ \lambda}{\beta\ \cos\theta} \tag{2}$$

where K is the shape constant ($K = 0.94$) and β is the width of the diffraction peak at half maximum intensity.

To evaluate the uniformity of the final channels' diameter, an imaging processing software was used to measure the perimeter and area, which were subsequently used to calculate the channel's

roundness using Equation 3:

$$\text{Roundness} = \frac{4\pi\text{Area}}{\text{Perimeter}^2}. \tag{3}$$

2.7. Mechanical testing

A three-point bending test was chosen for the manufactured and commercial samples due to its simplicity and ability to evaluate multiple tests in a short period of time. Tests were performed on an apparatus from Wyoming Fixtures^{TM} and done according to the ASTM D790 [34] standard. The loading nose and supports have a radii of 6 mm. The channel was perpendicular to the loading nose. Two Pike^{TM} F-505B cameras were used for 3D Stereo DIC (Digital Image Correlation) at a stereo-angle of 15°, and two AmScope^{TM} HL250-A were used for lighting the region of interest on the sample. A test figure is included in the supplementary information (Figure S2).

C/C composite commercial samples without channels (C/C-commercial), and C/C composite samples fabricated in this work without (C/C-no channel) and with channels (C/C-with channel) were cut into rectangular coupons on a Buehler^{TM} Isomet^{TM} 1000 precision saw. The dimensions of tested samples are given in Table 1.

A recommended support span-to-depth ratio of 16:1 was used to calculate the crosshead rate R, using Equation 4 [34]

$$R = \frac{ZL^2}{6d} \tag{4}$$

where R is the crosshead rate in mm/min, Z is the rate of straining of the outer fiber in mm/mm/min which is equal to 0.01, L is the support span in mm, and d is the depth of the sample in mm. The crosshead motion ranged from 1.28 to 1.64 mm/min. Flexural stress σ_f was calculated using Equation 5 [34]

$$\sigma_f = \frac{3PL}{2bd^2} \tag{5}$$

where P is the load in N, L is the support span in mm, b is the width of the sample in mm, and d is the depth of the sample in mm. Flexural strain ε_f was calculated using Equation 6 [34]

$$\varepsilon_f = \frac{6Dd}{L^2} \tag{6}$$

where D is the maximum deflection of the center of the sample in mm which was recorded from the loading nose and DIC, d is the thickness of the sample in mm, and L is the support span in mm. Flexural modulus E_o was calculated using Equation 7 [34]

$$E_o = \frac{L^3 m}{4bd^3} \tag{7}$$

where L is the support span in mm, m is the slope of the tangent to the initial straight-line portion of the load-deflection curve of deflection in N/mm, b is the width of the sample in mm, and d is the depth of the sample in mm.

A paired t-test was used to evaluate the flexural modulus and flexural strength data using the SciPy® library in Python® at a 95% confidence level.

3. Results and discussion

3.1. Cured prepregs with channels

To develop the procedure to fabricate prepregs with channels, PAN-based or pitch-based carbon fibers combined with pure and 10 wt% resorcinol-added phenolic resins were used. With an out-of-autoclave approach, the prepregs have a high void content, as shown in Figure 5(a). This behavior is attributed mostly to the formation of water vapor from the resin curing reactions. To obtain a prepreg with lower void content, an in-house designed autoclave was used in combination with a vacuum bag as described in section 2.2. The autoclave provides an external pressure (160 psi) to the vacuum bag that collapses and removes bubbles that are formed during the curing reactions, obtaining a void-free prepreg as shown in Figure 5(b). However, because curing of pure phenolic resins starts at around 80 °C, which is above the T_g (glass transition temperature) of PLA (52.4 °C), the compaction forces from the high pressure provided by the autoclave causes the channels to collapse and thus none are visible in the cured prepreg (Figure 5(b)).

Following our previous study on the curing kinetics of resorcinol-added phenolic resins[33], the addition of resorcinol can be used to allow B-stage curing to occur below the T_g (glass transition temperature) of PLA, as illustrated in Figure 6(a). The higher viscosity of the B-stage cured resin matrix provides enough resistance to the layup, preventing channel compaction while still taking advantage of the low void content provided by the use of an autoclave. As shown in Figure 6(b), 10 wt% resorcinol-added phenolic resin cured with the autoclave yields a prepreg

with very low void content and an intact channel. Next, the 3D printed PLA channels are removed by performing a heat treatment under vacuum at 290 °C for 24h, leaving a cleared channel network. In this work, channels of 500 μm in diameter, such as the one shown in Figure 3, were used to develop the fabrication procedure. It is to be noted that the same process can be followed for channels of smaller diameters and different design configurations, such as the feeder-header approach discussed in our previous work [8].

3.2. Carbonization and stress relief through graphitization

Prepregs with a cleared channel network were then carbonized at 1000 °C, following the procedure described in section 2.3. This process converts the resin into a continuous carbonaceous matrix, which at this point is mostly amorphous. Due to gas evolution, the specimen's density decreases and porosity increases. During the development of the fabrication procedure, it was observed that when graphitization was done only as a final step (i.e. skipping step 4 in Figure 2), delamination of the sample was a common occurrence, especially when PAN-based CF was used to produce the composite. It is hypothesized that, because the carbon matrix comes from two different sources (from phenolic resin and from CVI methane), residual stresses develop due to the mismatch of these carbon structures, which is supported by the XRD analysis to be discussed in section 3.4. PAN-based CF are also likely to undergo structural changes at 2200°C that further contribute to delamination, which is not the case when using the highly graphitic pitch-based CF. Thus, by performing an intermediate graphitization step (step 4 in Figure 2), these stresses are relieved by graphitizing the carbon matrix from the resin, preventing delamination to occur in the subsequent fabrication steps (steps 5 and 6 in Figure 2). This intermediate graphitization step is also characterized by a slight increase in density and open porosity due to the changes in the matrix from an amorphous type of carbon into a more crystalline graphitic structure.
SEM was used to evaluate the morphology of the fibers and carbon matrix of carbonized samples before (step 3 in Figure 2) and after (step 4 in Figure 2) the intermediate graphitization step, done at 2200 °C for 1 hour. As shown in Figure 7, the specimen shows a change in morphology from carbonization (a) to being graphitized (b), which can also be a contributing factor to the previously observed delamination issues.

3.3. Densification through CVI

To fill the pores of the composite, CVI was done using methane at 1000 °C and 200 mbar, as described in section 2.4. Densities were taken after 20-hour cycles to evaluate the increase in weight. Through cracking of methane at 1000 °C, carbon is slowly deposited into the interior pores of the composite. The density of the composite is increased as a direct results of the CVI procedure, which fills the pores with carbon. This phenomenon can be observed through SEM imaging, as shown in Figure 8. The different carbon sources can be differentiated, where the carbon matrix from the resin surrounds the fibers as the matrix shrinks towards the fibers during carbonization, causing the formation of pores, and the carbon from CVI tends to accumulate at the surface of the pores. The increase in density is a direct effect of the pores of the material being filled with deposited carbon from CVI. As shown in Figure 8, the pore-filling effect from CVI can be observed through SEM imaging, where the different sources of carbon can be differentiated, where the resin carbon presents itself in a stacked morphology due to the graphitization heat treatment, while the CVI carbon is slowly deposited at 1000 °C.
Figure 9 shows the changes in density and porosity, measured using the water absorption method. These results show the progression for the fabrication steps from 3 through 6, as indicated in Figure 2. The intermediate graphitization step (from 3 to 4) shows an increase in porosity for the sample prepared using PAN-based CF. These carbon fibers have a lower carbon content compared to pitch-based CF (93 and 99 wt%, respectively), as well as a lower graphitization degree, which likely contribute to opening isolated closed pores when heat treated at 2200 °C, thus increasing porosity. For C/C composites prepared using PAN or pitch-based CF, there is a clear increase in density and decrease in porosity due to the densification procedure, achieving a final density and porosity of 1.64 g/cm^3 and 4.9% for PAN-based, and 1.66 g/cm^3 and 10% for pitch-based, respectively, which are comparable to results reported in the literature [23, 24] as shown in Figure 9. As discussed in section 3.5, the CVI densification method does not clog the channels, while the overall density of the C/C composite increased.

3.4. XRD analysis for each fabrication step

To evaluate the effect of the different heat treatments on the composite, XRD analysis was done on the cross-section of samples for five different fabrication stages. Figure 10 summarizes the results for C/C composites fabricated using PAN-based carbon fibers. In addition to the steps

shown in Figure 2, an extra graphitization step for 6 hours was performed to evaluate the effect of a longer heat treatment on the graphitization degree of the composite. When evaluating the XRD results, the (002) peak is used since it is the most prominent and sensitive to changes in the crystalline structures, as opposed to the (101) and (004) reflections. In Figure 10(a), a clear difference between the carbonized and the first graphitization step is observed, where the (002) peak goes from being wider and lower to higher and sharper, suggesting a transition from an amorphous carbon structure to a crystalline graphitic one [35]. Isolating the (002) peak detail (Figure 10(b)), this difference is clearer. However, for all the subsequent steps after the first graphitization, the peaks do not show a significant change. During the CVI densification, deposited carbon should be mostly amorphous and the slightly lower and wider peak observed (Figure 10(b)) likely confirms this assumption. But since most of the carbonaceous matrix comes from the resin, which at this point (in step 5) is already graphitized, this change in the peak width and height is expected to be small.

XRD analysis was also done using isolated PAN-based carbon fibers and isolated matrix in a powdered form, to study the potential changes for each component. Figure 11(a) shows the XRD progression as each heat treatment was performed, with the exception of the CVI densification step. The carbonized (i.e. heat treated at 1000 °C in nitrogen atmosphere) PAN-based CF displayed a significant amorphous nature, with its (002) peak being wide and shallow. In Figure 11(b), after 1 hour of graphitization, the peak becomes more crystalline, reaching peak sharpness after 3 hours of graphitization. This behaviour suggests that the fibers undergo structural changes during graphitization, which can be another reason why delamination of the composite is sometimes present when the intermediate graphitization step (step 4 in Figure 2) is skipped. Figure 12(a) shows the same heat treatment results but for the matrix, which was prepared from resorcinol-added phenolic resin cured at 160 °C and powdered after carbonization at 1000 °C under nitrogen. Similar to the PAN-based CF, the carbonized matrix displays an amorphous nature with increased crystallinity after 1 hour of graphitization, shown by the (002) peak becoming sharper in Figure 12(b). The subsequent graphitization heat treatment steps (3h and the additional 6h at 2200 °C) do not seem to contribute to an increase in crystallinity. The XRD of the PAN-based CF and the matrix suggests that the additional 6 hours of graphitization at 2200 °C is not necessary to achieve the maximum graphitization degree possible at this temperature. Although the 3 hours of graphitization (step 6 in Figure 2) does not appear to

change the crystallinity of the matrix as shown in Figure 12, it does increase the graphitization degree of the PAN-based CF, and thus is a recommended step.

Carbon/carbon composite samples were also prepared using pitch-based CF, using the same fabrication procedure described in sections 2.2 to 2.5 and shown in Figure 2. These samples were then cross sectioned and analysed with XRD, as well as the isolated pitch-based CF. Unlike the PAN-based CF, there was no significant difference in the XRD results for each heat treatment step, as shown in Figure 13(a). Figure 13(b) shows that the pitch-based CF are highly graphitic, which suggests that the graphitic (002) peak from the fibers are so prominent that it masks the amorphous contribution from the matrix (Figure 12). Thus, similar to the PAN-based C/C composites, the composites prepared with pitch-based CF do not require the extra 6h of graphitization. These results may also suggest that the 3 hours of graphitization is not necessary, however they do not account for the presence of the amorphous carbon from the CVI densification. Thus, the final 3 hours of graphitization is required in order to ensure the graphitization of the carbon from the CVI procedure.

To obtain an approximation of graphitization degree, it was assumed that the amorphous carbon does not contribute to the (002) peak height, but rather only to the background pattern [36, 37]. The crystalline percentage can thus be calculated by using the ratio between the peak height from the baseline, and the baseline height at the 2θ peak, as illustrated in Figure 14 and shown in Equation 8, where I indicates the intensity at the (002) peak's position. In addition, the crystallite size can also be calculated using the Scherrer's equation (Equation 2), where an increase in L will indicate the presence of larger graphitic crystals and thus a higher degree of graphitization.

$$\text{Crystallinity}[\%] = \frac{I_{(002)} - I_{\text{Amorphous}}}{I_{(002)}} \times 100. \tag{8}$$

For each sample analyzed by XRD, crystallite size and crystallinity degree were calculated and results are summarized in Figure 15, where the "fabrication step n" refers to the steps shown in Figure 2, with the exception of step 7 which refers to the additional graphitization of 6h done to evaluate the effect of longer heat treatment at the end. A table containing the calculated values, as well as the d-spacing, is available as supplementary information. Figure 15(a) shows that for the matrix and the PAN-based CF and C/C composites, the carbonization step has the smallest crystallite size which progressively increases with each heat treatment. The pitch-based CF has a

significantly larger crystallite size, while the C/C composites prepared using these fibers show a decrease in crystallite size in comparison. This confirms that the matrix is indeed not as crystalline as the pitch-based carbon fibers, but the composite still benefits from the high graphitization degree of the pitch-based CF. The graphitization progression becomes more evident and easier to understand when evaluating the crystallinity percentage, as shown in Figure 15 (b). For the matrix, C/C composites prepared with PAN-based CF, and the PAN-based CF, the crystallinity jumps from around 55% after carbonization, to above 80 % after the first graphitization step (step 4 in Figure 2). As expected, the isolated pitch-based CF and the C/C composites prepared with these fibers exhibit the highest crystallinity percentage, all staying above 99%. Although these crystalline percentages are an approximation, they do give important insight into the effect of the high-temperature treatment to achieve graphitization, allowing this step to be optimized for the necessary number of times and duration of heat treatments.
The through-plane thermal conductivity of C/C composites fabricated in this work using PAN-based carbon fibers and a commercial sample (Across Inc.) was reported in our previous work, with values of 0.6 W m^{-1} K^{-1} and 15 0.6 W m^{-1} K^{-1} respectively [8]. In this work, a measurement of thermal conductivity was performed for samples prepared with pitch-based CF (not previously reported), with a recorded value of 13.0 W m^{-1} K^{-1}. The through-plane thermal conductivity is notably influenced by the matrix properties; however, the incorporation of highly graphitic pitch-based carbon fibers greatly increases thermal conductivity, being very close to the values measured for the commercial sample, shown here as a baseline for comparison. This shows that the fabrication procedure developed in this work can maintain the high thermal conductivity characteristic of C/C composites.

3.5. Channels of C/C composite samples

The finalized carbon/carbon composites with channels were sectioned and analyzed using SEM. When using woven layers of PAN-based carbon fibers to produce C/C composites, the channels tend to be squished (0.61 roundness), showing a more oblong shape rather than the original circular one, as shown in Figure 16(a). Channel fidelity was improved by using a mixed-layered approach to fabricate the composites, increasing the final roundness of the channel diameter to 0.77. In this case, the PLA channels were placed in between 4 layers of unidirectional carbon fibers running in the same direction. As the fibers run parallel to the PLA channel, they can maintain their shape by better redistributing the compaction forces. To provide extra support

and strength to the final material, 3 woven layers were placed on top and at the bottom of the unidirectional fibers. As shown in Figure 16(b), this approach produces channels that have better channel fidelity to the original PLA template. A similar behaviour is observed when using pitch-based carbon fibers to produce the composites, as shown in 16(c) for woven fibers (roundness of 0.56), and in 16(d) for mixed-layered with unidirectional fibers running parallel to the channels (roundness of 0.72).

To evaluate the condition of the channels, NanoCT analysis was done in a sample with one single straight channel. Figure 17 shows the NanoCT images, where the channels are completely cleared, confirming that the fabrication approach developed in this work is able to deliver unobstructed channels.

3.6. Mechanical testing

Flexural modulus was calculated using Equation 7 and deflection from the loading nose and from the DIC region of interest. A representative load-displacement curve from the load frame and DIC that was used to calculate the mechanical properties is included in the supplementary information (Figures S3 and S4). The results, in Figure 18(a), show a clear difference in flexural modulus calculated using deflection values from the crosshead and from the DIC region of interest. The difference is 25.74%, 20.38% and 16.67% for C/C-commercial, C/C-no channel and C/C-with channel respectively. Given this disparity, the properties derived from the displacement recorded by the DIC system are reported, as recommended by ASTM D790 [34].

The flexural strength was calculated using Equation 5. The results are shown in Figure 18(b). The C/C composite samples fabricated in this work had a higher flexural strength than the commercial samples, which can be attributed to the differences in CF type, layup configuration, and fabrication method.

Table 3 summarises the mechanical properties of the samples prepared in this study. The flexural strength and flexural modulus for the C/C-commercial compares to the 180 MPa and 45 GPa reported by the manufacturer Across USA, Inc. This result provides confidence in the experimental setup and data obtained for the C/C composite samples fabricated in this work with and without a channel. To better quantify the influence of a straight channel on the mechanical properties of a C/C composite sample, a paired t-test of the flexural strength and flexural modulus of C/C-no channel and C/C-with channel was applied. A p-value of 0.6219 and 0.2798 at a 95% confidence level indicate that there is no statistically significant difference in the

flexural strength and flexural modulus C/C composite samples fabricated either with or without channels. This result is somewhat unsurprising, as the channels are located along the midplane of the specimen, where the stresses are low. The results are presented for longitudinal orientation of the channel in the composite. Transverse orientation will likely result in reductions in ultimate bending strengths. The complete mechanical performance of the vascular composite will be reported in a forthcoming paper.

4. Conclusions

An experimental procedure to produce a novel C/C composite with channels was developed. Since the use of only vacuum bag for curing was not effective, an in-house designed autoclave was used to produce prepregs with very low void content. Due to the high compaction forces provided by the high pressure autoclave, the PLA channel on these samples were flattened. This problem was solved by using resorcinol-added phenolic resin, which allows for the resin to be B-stage cured below the glass transition temperature of the PLA channel, maintaining the channel's integrity during the curing procedure. Depolymerization of the prepregs removes the PLA channel mold, leaving behind the desired cleared channel network. Carbonization was done at 1000 °C to convert the resin matrix into a continuous carbonaceous matrix. It was also shown that an intermediate graphitization step right after carbonization helped in relieving residual stresses, preventing delamination issues during the subsequent heat treatments. Specimens were CVI densified and subsequently graphitized at 2200 °C. The XRD study showed that there is no significant increase in crystallinity for samples graphitized for an additional 6 hours, thus 3 hours of heat treatment was deemed sufficient. The mechanical testing revealed that the presence of channels has little detrimental effect on the flexural strength and flexural modulus of the C/C composite for this configuration.

Acknowledgements

The authors acknowledge the financial support for this work from the United States Department of Energy (DoE), Award No. DE-EE0008736.

References

[1] K. Lovegrove, W. Stein, Concentrating solar power technology: principles, developments and applications, 2012.

[2] S. Kuravi, J. Trahan, D. Y. Goswami, M. M. Rahman, E. K. Stefanakos, Thermal energy storage technologies and systems for concentrating solar power plants, Progress in Energy and Combustion Science 39 (4) (2013) 285–319. doi:10.1016/j.pecs.2013.02.001.

[3] M. Mehos, C. Turchi, J. Vidal, M. Wagner, Z. Ma, C. Ho, W. Kolb, C. Andraka, A. Kruizenga, Concentrating Solar Power Gen3 Demonstration Roadmap, Nrel/Tp-5500-67464 (January) (2017) 1–140. doi:10.2172/1338899.

[4] K. R. Zada, M. B. Hyder, M. Kevin Drost, B. M. Fronk, Numbering-Up of Microscale Devices for Megawatt-Scale Supercritical Carbon Dioxide Concentrating Solar Power Receivers, Journal of Solar Energy Engineering, Transactions of the ASME 138 (6) (2016) 1–9. doi:10.1115/1.4034516.

[5] J. N. Sweet, E. P. Roth, M. Moss, Thermal conductivity of Inconel 718 and 304 stainless steel, International Journal of Thermophysics 8 (5) (1987) 593–606. doi:10.1007/BF00503645.

[6] R. Luo, T. Liu, J. Li, H. Zhang, Z. Chen, G. Tian, Thermophysical properties of carbon/carbon composites and physical mechanism of thermal expansion and thermal conductivity, Carbon 42 (14) (2004) 2887–2895. doi:10.1016/j.carbon.2004.06.024.

[7] D. D. Chung, Carbon Fiber Composites, 2012. doi:10.1016/C2009-0-26078-8.

[8] M. Zuzelski, M. Laporte-Azcué, J. Cordeiro, S. Dhakal, V. Daghigh, M. Keller, H. Ramsurn, T. Otanicar, Design of a novel carbon/carbon composite microvascular solar receiver, Solar Energy 262 (2023) 111794. doi:10.1016/j.solener.2023.111794.

[9] S. Awasthi, J. L. Wood, Carbon/Carbon Composite Materials for Aircraft Brakes, Ceramic Engineering and Science Proceedings 560 (1988) 553–559. doi:10.1002/9780470310496.ch4.

[10] G. Savage, Carbon-Carbon Composites, Springer Netherlands, 1993.

[11] H. C. Shao, H. Y. Xia, G. W. Liu, G. J. Qiao, Z. C. Xiao, J. M. Su, X. H. Zhang, Y. J. Li, Densification Behavior and Performances of C/C Composites Derived from Various Carbon Matrix Precursors, Journal of Materials Engineering and Performance 23 (1) (2014) 133–141. doi:10.1007/s11665-013-0667-z.

[12] S.-S. Tzeng, J.-H. Pan, Densification of two-dimensional carbon/carbon composites by pitch impregnation, Materials Science and Engineering: A 316 (1-2) (2001) 127–134. doi:10.1016/S0921-5093(01)01255-2.

[13] L. Manocha, H. Bhatt, S. Manocha, Development of carbon/carbon composites by co-carbonization of phenolic resin and oxidised pan fibers, Carbon 34 (7) (1996) 841–849. doi:10.1016/0008-6223(95)00201-4.

[14] E. Fitzer, B. Terwiesch, Carbon—carbon composites unidirectionally reinforced with carbon and graphite fibers, Carbon 10 (4) (1972) 383–390. doi:10.1016/0008-6223(72)90053-X.

[15] T.-H. Ko, P.-C. Chen, Study of the pyrolysis of phenolic resin reinforced with two-dimensional plain woven carbon fabric-I, Journal of Materials Science Letters 10 (5) (1991) 301–303. doi:10.1007/BF00735665.

[16] W. Li, Z. Chen, J. Li, X. Chen, H. Xuan, X. Wang, Preparation of PAN/phenolic-based carbon/carbon composites with flexible towpreg carbon fiber, Materials Science and Engineering: A 485 (1-2) (2008) 481–486. doi:10.1016/j.msea.2007.08.017.

[17] I. Golecki, R. C. Morris, D. Narasimhan, N. Clements, Rapid densification of porous carbon-carbon

composites by thermal-gradient chemical vapor infiltration, Applied Physics Letters 2334 (1995) (1995) 2334. doi:10.1063/1.113974.

[18] B. Wielage, A. G. Odeshi, H. Mucha, H. Lang, R. Buschbeck, A cost effective route for the densification of carbon–carbon composites, Journal of Materials Processing Technology 132 (1-3) (2003) 313–322. doi:10.1016/S0924-0136(02)00951-2.

[19] T. Kajita, L. C. Pardini, F. C. L. de Melo, Chemical Vapor Densification Process of Carbon Fiber Substrates, Materials Science Forum 498-499 (2005) 413–419. doi:10.4028/www.scientific.net/msf.498-499.413.

[20] J. Chen, X. Xiong, Q. Huang, M. Yi, B. Huang, Densification mechanism of chemical vapor infiltration technology for carbon/carbon composites, Transactions of Nonferrous Metals Society of China 17 (3) (2007) 519–522. doi:10.1016/S1003-6326(07)60126-5.

[21] A. Dekeyrel, M. A. Dourges, P. Weisbecker, R. Pailler, A. Allemand, N. Ténèze, J. F. Epherre, Characterization of carbon/carbon composites prepared by different processing routes including liquid pitch densification process, Composites Part A: Applied Science and Manufacturingdoi:10.1016/j.compositesa.2013.02.010.

[22] M. Albano, R. Pastore, A. Delfini, D. Micheli, F. Volpini, M. Marchetti, Densification of High Thickness C/C Composites by Chemical Vapor Infiltration, in: Procedia Engineering, Vol. 109, Elsevier Ltd, 2015, pp. 381–389. doi:10.1016/j.proeng.2015.06.246.

[23] J. Ren, K. Li, S. Zhang, X. Yao, S. Tian, Preparation of carbon/carbon composite by pyrolysis of ethanol and methane, Materials & Design (1980-2015) 65 (2015) 174–178. doi:10.1016/J.MATDES.2014.08.036.

[24] X. Zhang, X. Li, G. Yuan, Z. Dong, G. Ma, B. Rand, Large diameter pitch-based graphite fiber reinforced unidirectional carbon/carbon composites with high thermal conductivity densified by chemical vapor infiltration, Carbon 114 (2017) 59–69. doi:10.1016/j.carbon.2016.11.080.

[25] A. Sedghi, F. G. Fard, The effect of Graphitization on the Mechanical Properties of twodimensional carbon - carbon composites, Materialwissenschaft und Werkstofftechnik 28 (5) (1997) 236–240. doi:10.1002/mawe.19970280510.

[26] K. Matsui, L. J. Lanticse, Y. Tanabe, E. Yasuda, M. Endo, Stress graphitization of C/C composite reinforced by carbon nanofiber, Carbon 43 (7) (2005) 1577–1579. doi:10.1016/j.carbon.2005.01.034.

[27] A. P. Esser-Kahn, P. R. Thakre, H. Dong, J. F. Patrick, V. K. Vlasko-Vlasov, N. R. Sottos, J. S. Moore, S. R. White, Three-Dimensional Microvascular Fiber-Reinforced Composites, Advanced Materials 23 (32) (2011) 3654–3658. doi:10.1002/adma.201100933.

[28] A. M. Coppola, P. R. Thakre, N. R. Sottos, S. R. White, Tensile properties and damage evolution in vascular 3D woven glass/epoxy composites, Composites Part A: Applied Science and Manufacturing 59 (2014) 9–17.

[29] S. Olugebefola, A. Aragón, C. Hansen, A. Hamilton, B. Kozola, W. Wu, P. Geubelle, J. Lewis, N. Sottos, S. White, Polymer Microvascular Network Composites, Journal of Composite Materials 44 (22) (2010) 2587–2603. doi:10.1177/0021998310371537.

[30] S. J. Pety, M. H. Y. Tan, A. R. Najafi, P. R. Barnett, P. H. Geubelle, S. R. White, Carbon fiber composites with 2D microvascular networks for battery cooling, International Journal of Heat and Mass Transfer 115 (2017) 513–522. doi:10.1016/j.ijheatmasstransfer.2017.07.047.

[31] D. T. Bunce, K. P. Bassett, A. R. M. Ghosh, P. R. Barnett, D. M. Haken, S. Vrkljan, R. Jagannatha,

T. Silva, V. L. Coverstone, Microvascular Composite Radiators for Small Spacecraft Thermal Management Systems, 30th Annual AIAA/USU Conference on Small Satellites (2016) SSC16–X–1.

[32] M.-U. Saeed, Z. Chen, B. Li, Manufacturing strategies for microvascular polymeric composites: A review, Composites Part A: Applied Science and Manufacturing 78 (2015) 327–340.

[33] J. C. Cordeiro, R. E. Davis, H. Ramsurn, D. W. Crunkleton, T. P. Otanicar, M. W. Keller, Prediction of curing kinetics of resorcinol-added resole phenolic resins using differential scanning calorimetry for the fabrication of carbon/carbon composites, Journal of Applied Polymer Science 139 (39). doi:10.1002/app.52949.

[34] S. ASTM, Standard test methods for flexural properties of unreinforced and reinforced plastics and electrical insulating materials. ASTM D790, Annual book of ASTM Standards.

[35] Z. Li, C. Lu, Z. Xia, Y. Zhou, Z. Luo, X-ray diffraction patterns of graphite and turbostratic carbon, Carbon 45 (8) (2007) 1686–1695. doi:10.1016/j.carbon.2007.03.038.

[36] R. E. Franklin, Crystallite growth in graphitizing and non-graphitizing carbons, Proceedings of the Royal Society of London. Series A. Mathematical and Physical Sciences 209 (1097) (1951) 196–218.

[37] D.-S. Kang, S.-M. Lee, S.-H. Lee, J.-S. Roh, X-ray diffraction analysis of the crystallinity of phenolic resin-derived carbon as a function of the heating rate during the carbonization process, Carbon letters 27 (2018) 108–111.

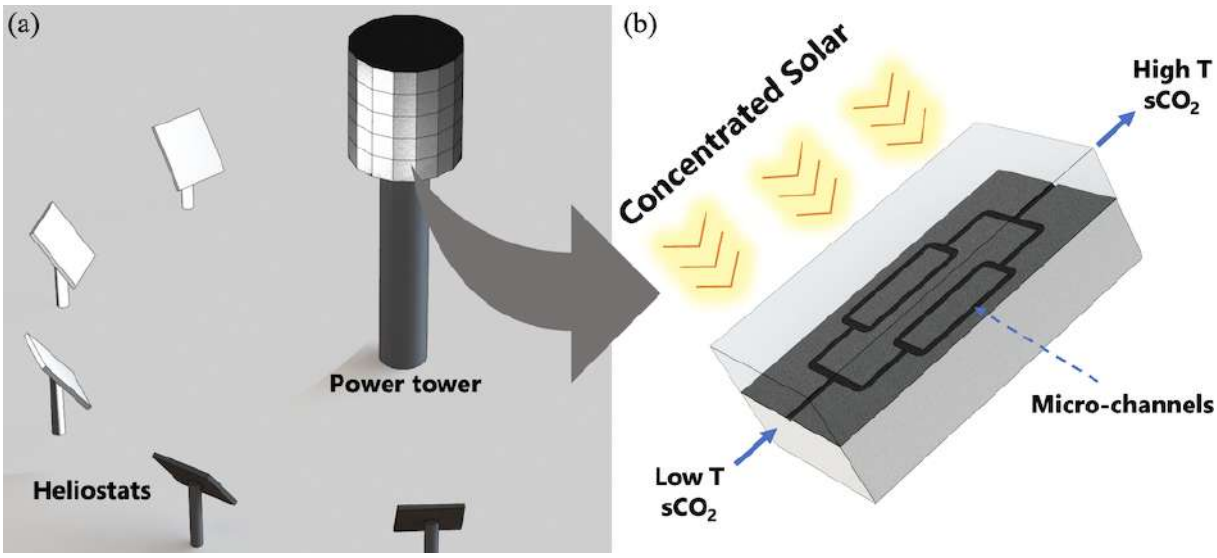

Figure 1: Proposed (a) concentrated solar power gas receiver with a (b) novel C/C composite with micro-channels in a modular configuration.

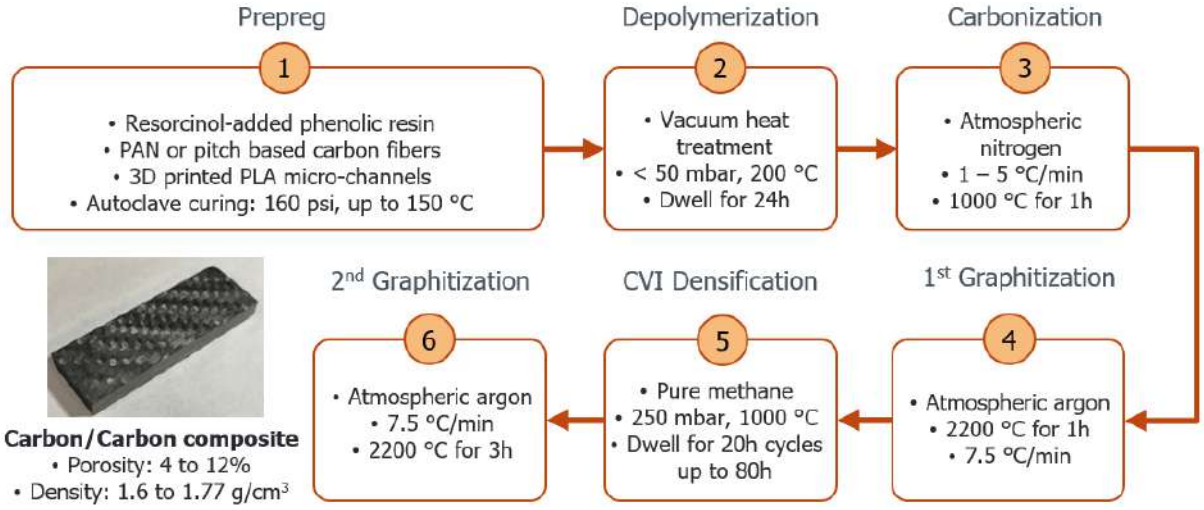

Figure 2: Steps and processing parameters for the fabrication of the novel C/C composites with embedded micro-channels.

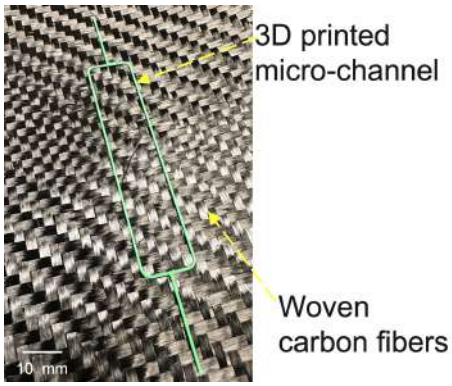

Figure 3: Example of a 3D printed PLA micro-channel template placed in between layers of woven carbon fiber.

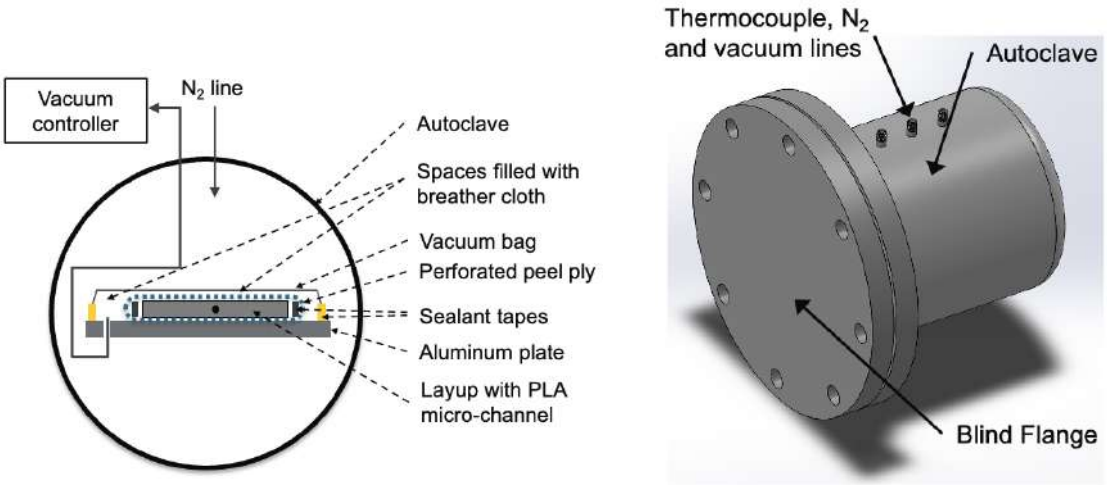

(a) (b)

Figure 4: (a) Front view schematic of prepreg curing and (b) in-house designed autoclave.

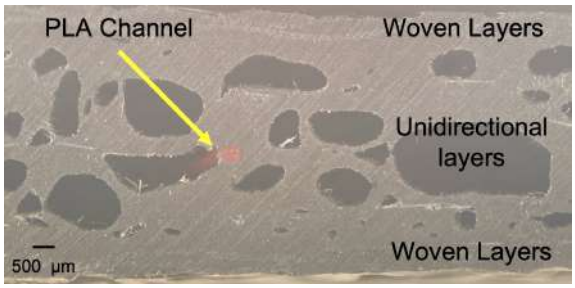

(a) Out-of-autoclave

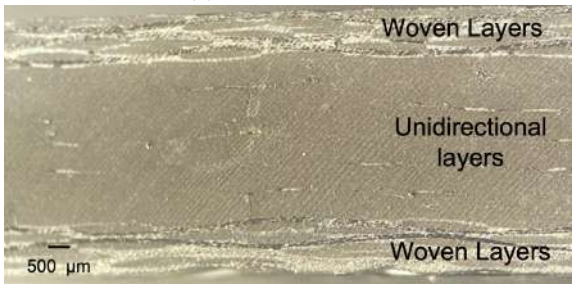

(b) In autoclave

Figure 5: Comparison between (a) out-of-autoclave and (b) autoclave curing procedures.

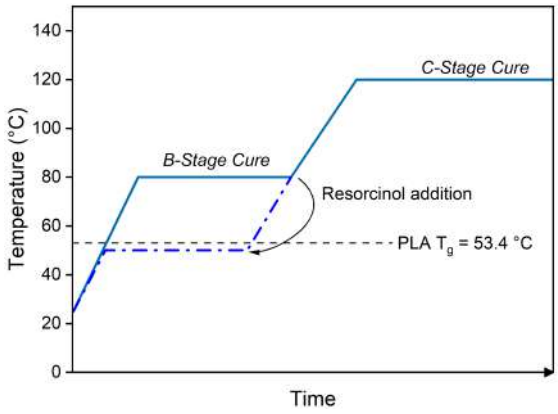

(a) Out-of-autoclave

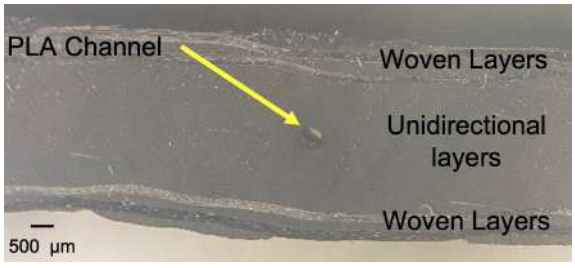

(b) In autoclave

Figure 6: (a) Resorcinol addition to decrease the B-stage curing temperature of phenolic resins, and (b) cured prepreg produced with 10 wt% resorcinol-added phenolic resin.

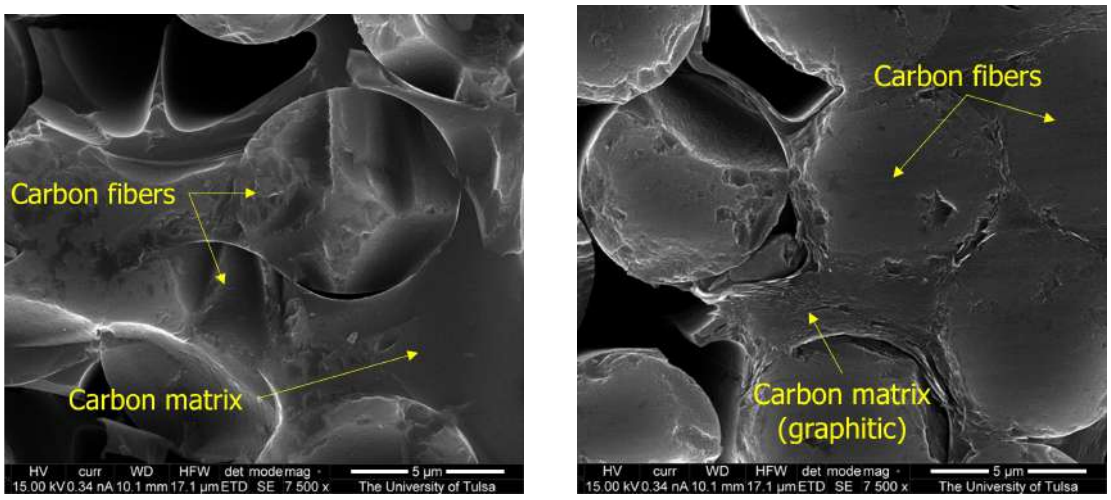

(a) (b)

Figure 7: SEM images of carbonized samples, (b) before and (b) after graphitization at 2200 °for 1 hour.

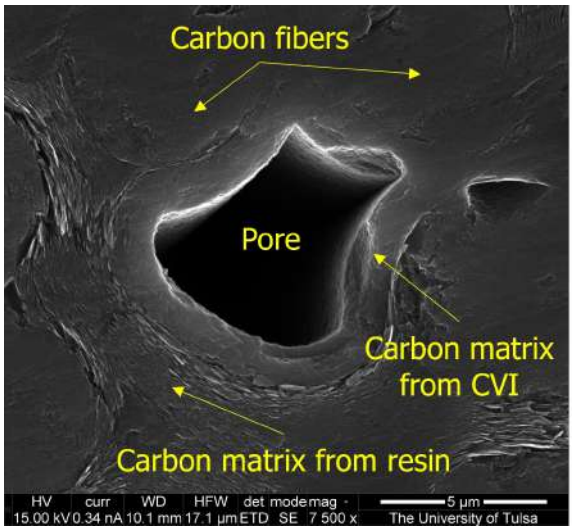

Figure 8: SEM imaging of the cross-section of a CVI densified sample, showing the carbon from the resin and from CVI.

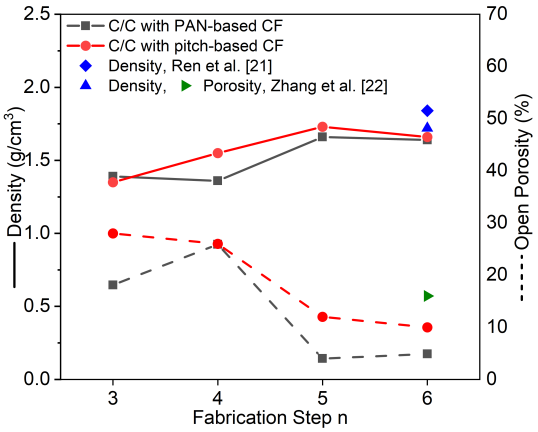

Figure 9: Porosity (SD $<$ 0.2 %) and density (SD $<$ 0.02 g/cm^3) results for C/C composites prepared with PAN and pitch-based CF and compared with literature data. The fabrication step n corresponds to the steps in Figure 2.

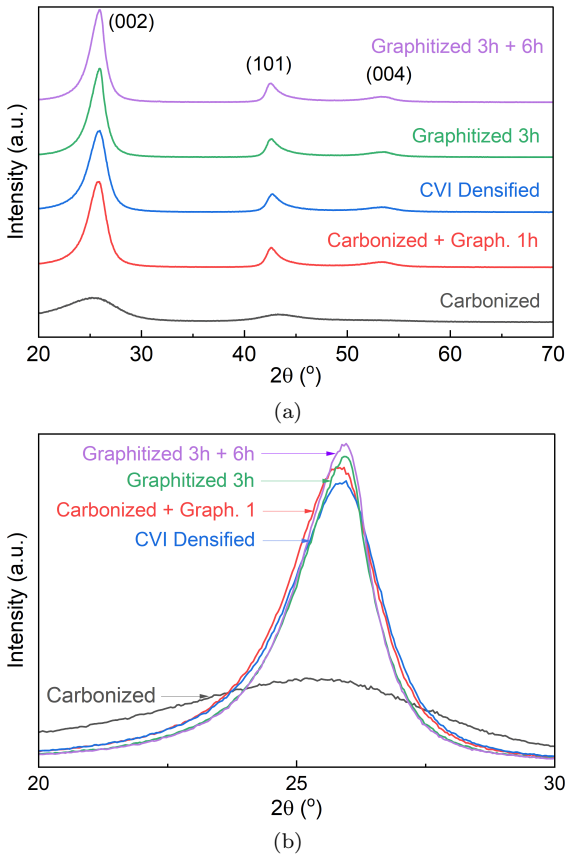

Figure 10: XRD results (a) for each fabrication step for C/C composites prepared using PAN-based carbon fibers, with (b) details on the (002) peak.

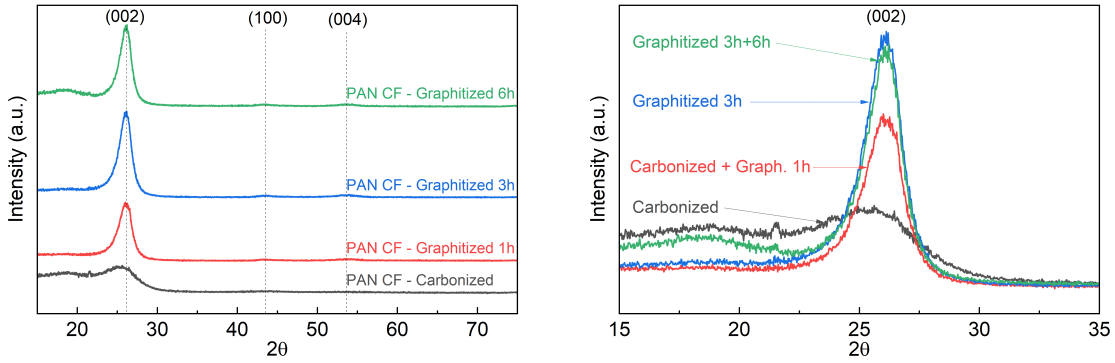

Figure 11: XRD results (a) for each fabrication step for PAN-based carbon fibers only, with (b) details on the (002) peak.

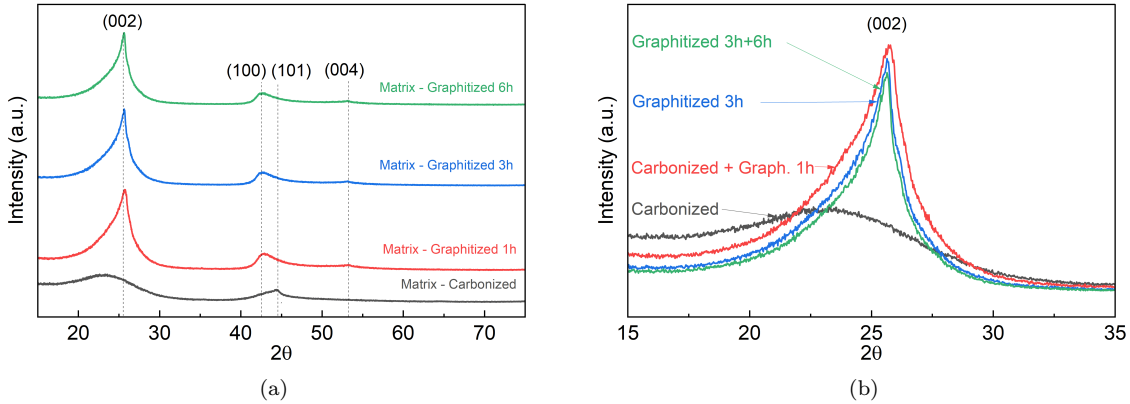

Figure 12: XRD results (a) for each fabrication step for the matrix only (resorcinol-added phenolic resin), with (b) details on the (002) peak.

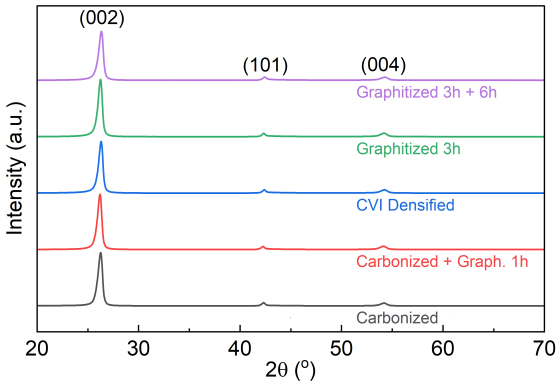

(a)

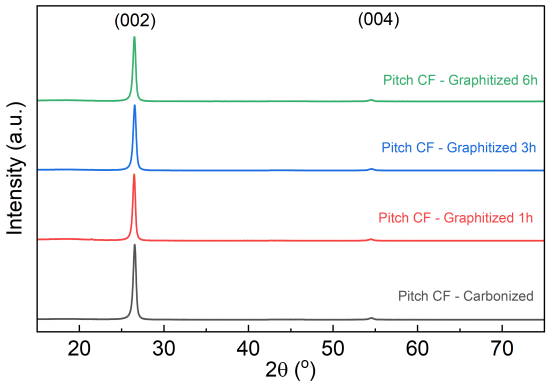

(b)

Figure 13: XRD results for each fabrication step for (a) C/C composites prepared with pitch-based carbon fibers and (b) pitch-based carbon fibers only.

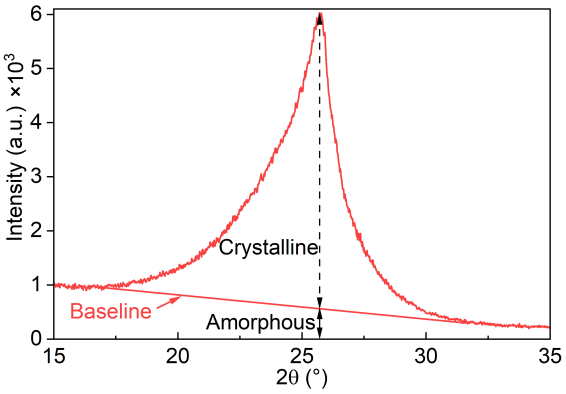

Figure 14: Example of the determination of crystalline percentage using the (002) peak height and subtracting its baseline. The example shown is for the matrix carbonized and graphitized for 1 hour.

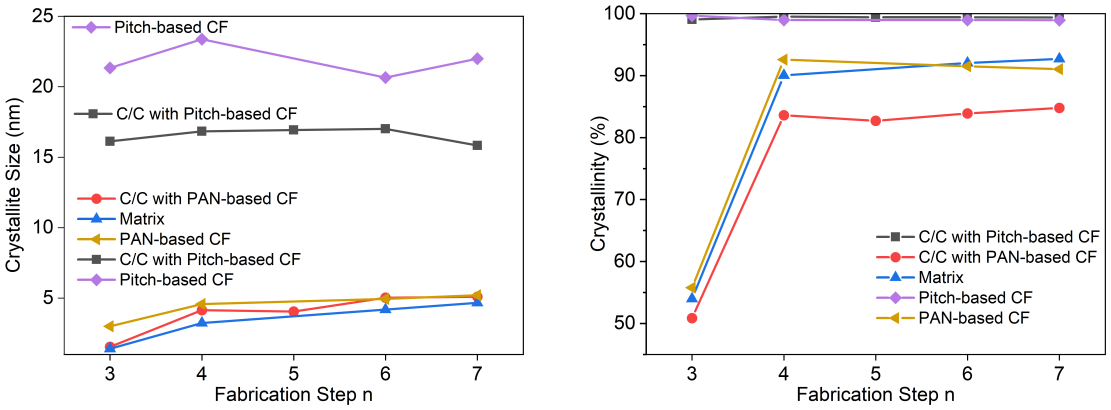

(a) (b)

Figure 15: (a) Crystallinity and (b) crystallite size for each fabrication step, as defined in Figure 2.

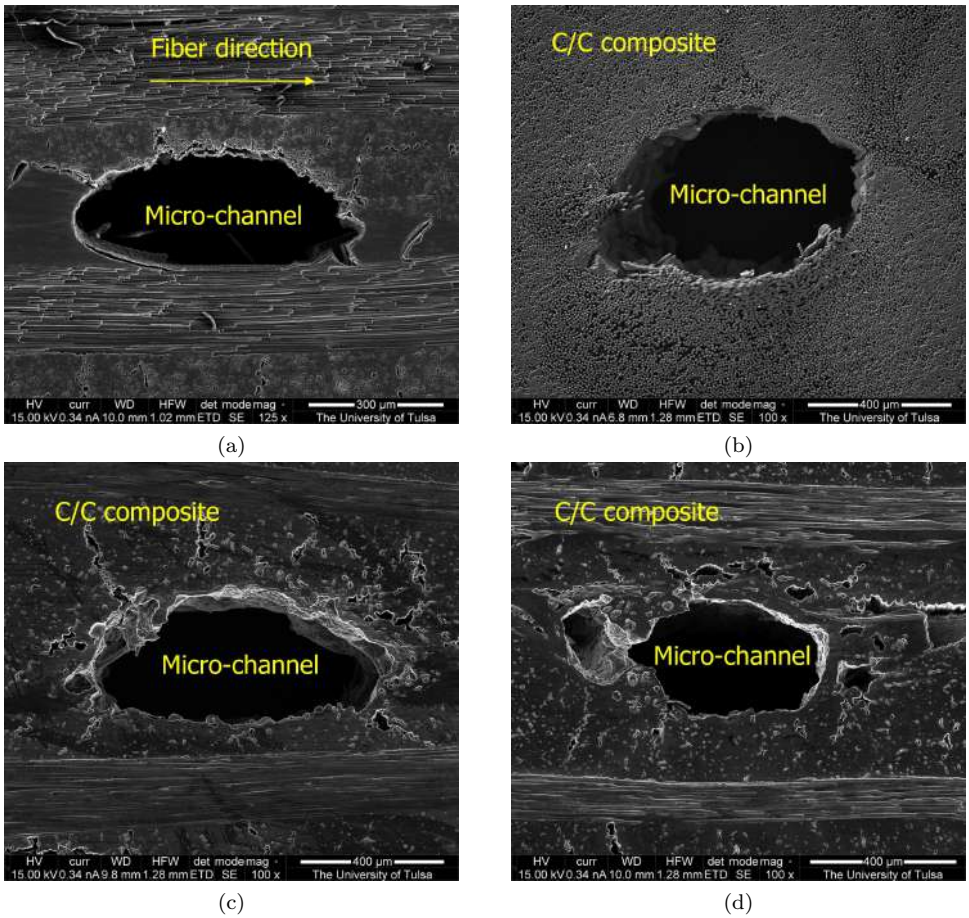

(a) (b)

(c) (d)

Figure 16: Micro-channels of C/C composites prepared using (a) woven PAN-based CF, (b) mixed PAN-based CF, (c) woven pitch-based CF, and (d) mixed pitch-based CF.

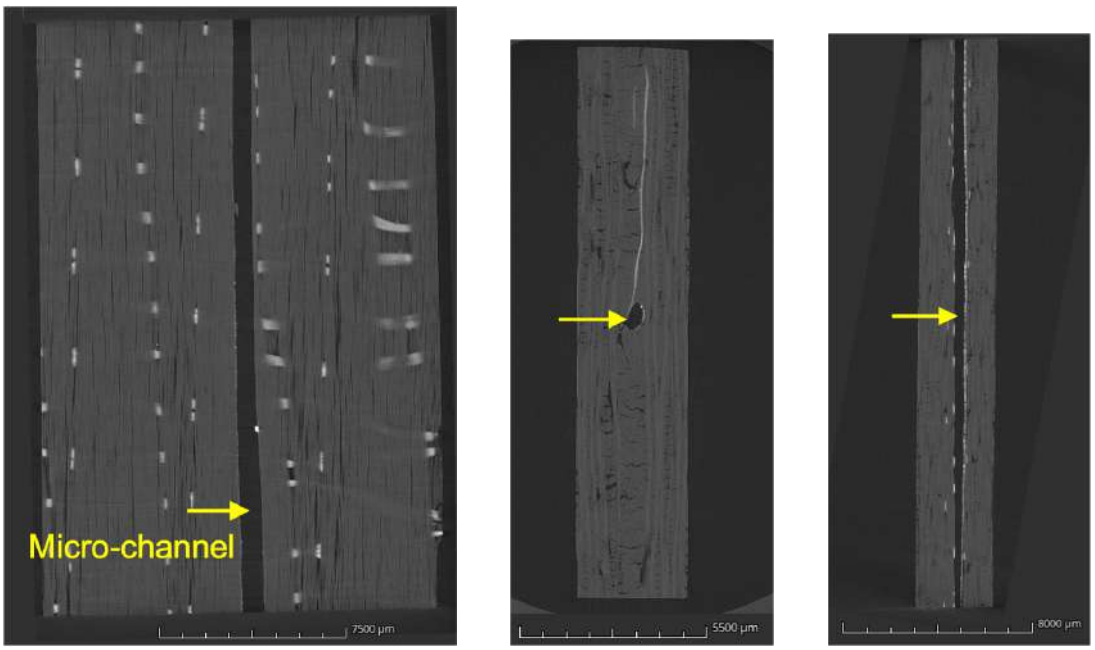

(a) (b) (c)

Figure 17: NanoCT images of a C/C composite sample prepared in this work, detailing the micro-channel from the (a) front, (b) side, and (c) top of the sample. The arrow indicates the cleared micro-channel.

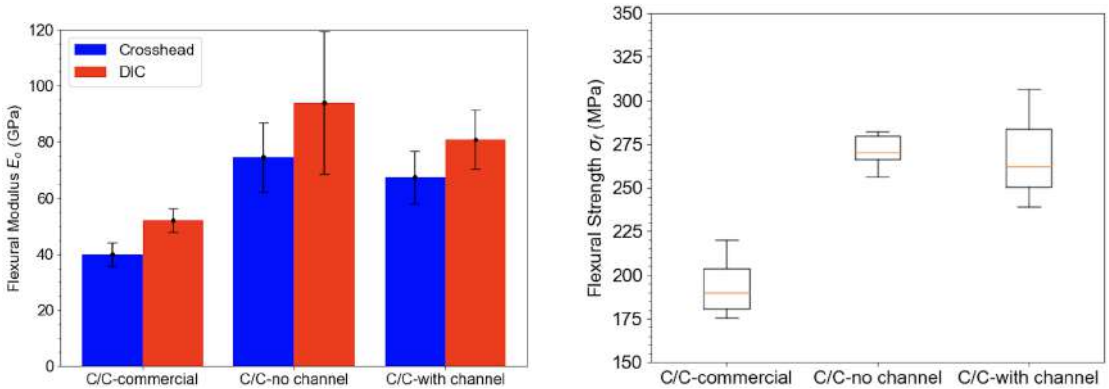

(a) (b)

Figure 18: (a) Flexural modulus of C/C composite samples under three-point bending loads using crosshead and DIC, and (b) flexural strength of C/C composite samples using DIC.

Table 1: Test sample dimensions.

	C/C-commercial	C/C-no channel	C/C-with channel
Tested	6	6	6
Thickness (mm)	3.01 ±0.01	3.53 ±0.32	3.52 ±0.26
Width (mm)	13.00 ±0.34	12.91 ±0.17	13.23 ±0.44
Length (mm)	101 ±1	101 ±1	101 ±1
Layers	7	14	14

Table 2: Mechanical properties of C/C samples from the flexural tests.

	C/C-commercial	C/C-no channel	C/C-with channel
Flexural strength (MPa)	193.64±17.51	274.78±15.11	267.94±25.73
Flexural modulus (GPa)	39.88±4.12	74.48±12.36	67.39±9.39